Pergamon

Journal of Structural Geology, Vol. 18, Nos 2/3, pp. 359 to 372, 1996

0191-8141/96 $15.00 + 0.00

0191-8141(95)00089-5

Spatial and mechanical controls on normal fault populations

STEVEN D. KNOTT,* ALASTAIR BEACH, PAUL J. BROCKBANK, J. LAWSON BROWN, JEAN E. McCALLUM and ALASTAIR I. WELBON

Alastair Beach Associates Ltd, 11 Royal Exchange Square, Glasgow G1 3AJ, Scotland, U.K.

(*Received* 25 *January* 1995; *accepted in revised form* 2 *July* 1995)

Abstract—Characteristics of normal faults have been measured from outcrops in western Sinai and northern Britain, and from the subsurface in the North Sea basin. Fault damage zone widths and the spatial distribution of minor structures around faults have been related to variation in throw along a fault surface. Secondary shear fractures, including faults and granulation seams, are most common within damage zone envelopes, in the immediate footwall and hangingwall, in the extensional field of major normal faults. Shear fractures are less common in the contractional field of normal faulted rock volumes. Fault zone thickness measurements from outcrop indicate scale invariance over several orders of magnitude within the same location and lithology. Fault zone thickness is linearly correlated to fault throw. There is a strong mechanical and lithological control on fault zone thickness. Coarse sandstones have thicker fault zones for a given throw, due to the processes of strain hardening and cataclasis, compared with argillaceous rocks which are prone to strain softening. Fault spacing in siliciclastic rocks can show scale invariance over several orders of magnitude. The influence of grain size and layer thickness on fault growth can lead to either non-fractal behaviour or changes in the power law for fault characteristics such as throw, thickness and spacing.

INTRODUCTION

Systematic analysis of fault characteristics includes studies of fault displacement (Barnett *et al.* 1987, Walsh & Watterson 1988a, Walsh *et al.* 1994), dip (Walsh & Watterson 1988b), fault length (Walsh & Watterson 1988a, Heffer & Bevan 1990, Marrett & Allmendinger 1991), fault spacing (Gillespie *et al.* 1993, Westaway 1994), linkage (Peacock & Sanderson 1991), structural compartmentalization (Gaultier & Lake 1993) and fault growth (Watterson 1986, Marrett & Allmendinger 1991, Cowie & Scholz 1992). Application of techniques derived from these analyses has revolutionized the assessment of complex structures in resource management. The usefulness and application of these techniques is based on the ability to predict, in a probabilistic sense, fault characteristics of a particular data set beyond the scale of observation (Childs *et al.* 1990).

Much progress has been made in recent years in understanding *how many* faults are present below the limit of resolution, particularly in the case of reflection seismic data (e.g. Yielding *et al.* 1992). However, it is only very recently that attention has been turned to *where* faults are located below the limit of resolution—whether the limit be in seismic, borehole image, or outcrop data. Progress has been made in estimating the number of faults within a range of sizes (e.g. Childs *et al.* 1990, Marrett & Allmendinger 1991, Gaultier & Lake 1993), but further work is required to more fully quantify what controls the position of faults within the faulted volume. Mechanical and lithological controls on fault growth and fault characteristics are still expanding areas of research (Watterson 1986, Cowie & Scholz 1992, Dawers *et al.* 1993).

We present the results of analysis of new data sets of outcrop and subsurface fault characteristics with particular emphasis on fault damage zone width, fault zone thickness and fault spacing, in order to gain a better understanding of what controls the spatial distribution of faults as well as the mechanical controls on fault populations.

FAULT CHARACTERISTICS

A fractal, or self-similar, population exists if the frequency of the individuals within the population remains constant over a range of sizes. One possible control on fault populations is their growth according to a power law relationship, such that under ideal conditions fault characteristics are self-similar for a range of sizes (King 1983, Watterson 1986). Fault-growth models offer a description of time-averaged behaviour which natural faults display only in a statistical way. The instantaneous characteristics of faults, at a point in time during their growth, may be quite different from the average view. Other controls on fault growth include the spatial variation in strain within the faulted volume, lithological variations such as grain size and layer thickness, and the mechanical properties of the faulted rocks. These controls are significant and have important implications for the prediction of fault characteristics in the subsurface.

We first describe data on damage zone widths, throws,

*To whom correspondence should be addressed.

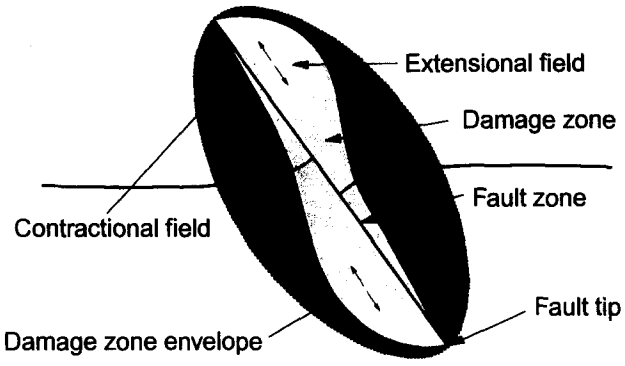

Fig. 1. Cartoon depicting cross-sectional damage zone geometry based on outcrop data. The damage zone is widest in the extensional field and narrowest in the contractional field. Damage zone width increases with increasing fault throw. Based in part on Muraoka & Kamata (1983) and Barnett *et al.* (1987) and outcrop data presented in Table 1.

lengths and thicknesses measured in outcrop and the subsurface which demonstrate, as has been shown in other studies, that fault populations are statistically self-similar. Aspects presented here that are different from previous work (Walsh & Watterson 1988a,b, Marrett & Allmendinger 1991, Yielding *et al.* 1992) include: (1) presentation of subsurface data from seismically derived structure maps of a well-imaged normal fault pattern from the Jurassic of the North Sea and a large data set of fracture characteristics measured from core, and (2) outcrop data from excellently exposed normal faults in western Sinai.

Fault damage zones

Faults in sandstone-rich rocks generally have an enveloping volume of small-scale structures around them which include faults and granulation seams, which may damage or enhance reservoir properties such as porosity and permeability, depending on whether the fractures are sealing or open to fluid flow respectively. Faults that we studied in outcrop are generally planar, have throws from 1 mm to several km, and have a normal sense of offset.

The deformed rock volume around a master fault is called the damage zone (Chester & Logan 1986, Koestler *et al.* 1994) (Fig. 1). Deformation in the damage zone occurs during fault-tip propagation and during slip on the master fault surface. Our outcrop studies show that the width of the damage zone, measured normal to fault strike, is greatest in the extensional field of a normal fault (Table 1). The widest damage zone for normal faults forms either in the hangingwall near the upper tip of the fault or in the footwall near the deeper tip (Fig. 1). By measuring faults of different sizes, we attempted to gain a general understanding of damage zone development. Even though the outcrop examples are individual sanpshots in time, in combination they may indicate the general relationship between a growing fault and its surrounding damage zone.

At a much smaller size than the damage zone, the master fault zone (Fig. 1), where most of the slip across the fault has occurred, is usually where the reservoir is most affected by deformation and cementation. Commonly, the permeability of the fault zone is several orders of magnitude less than the undeformed reservoir (Randolph & Johnson 1989, Antonellini & Aydin 1994, Fowles & Burley 1994). We use the term fault zone thickness (Hull 1988, Evans 1990, Knott 1994) for the width measurement of this smaller size of deformation feature.

Table 1. Outcrop measurements of throw and associated damage zone widths from Northern Britain and western Sinai. Damage zone half-width is the width measured across one wall of the fault (footwall or hangingwall). The tensile and extensional fields for fault damage zones were determined based on the throw variation down the fault plane. If throw increased downwards at the outcrop, then the hangingwall was in the extensional field during active faulting and vice versa. Locations: (1) Ninety Fathom fault, Northumberland; (2) Lacy's Caves, Cumbria; (3) Abbott Moss Quarry, Cumbria; (4) Hilbre Island, Cheshire; (5) George Gill, Cumbria; (6) Wadi Feiran, W Sinai (Fig. 5a); (7) Gebel Musaba Salama, W Sinai; (8) Wadi Mukattab, W Sinai (Fig. 6b); (9) Gebel Musaba Salama; (10) Hilbre Island; (11) Hilbre Island

	Damage zone half-width (m)		
Throw (m)	Tensile field	Contractional field	Location
140	300		N Britain (1)
4	15	10	N Britain (2)
10	20	15	N Britain (3)
3	6		N Britain (4)
75	150		N Britain (5)
40	75		W Sinai (6)
50	60		W Sinai (7)
50		25	W Sinai (8)
100		40	W Sinai (9)
0.7	1.5		N Britain (10)
0.4	1		N Britain (11)

In order to define the widths of damage zones, we collected data on fractures in a general sense, i.e. both faults and joints, along linear traverses oriented normal to the trends of well-exposed faults in western Sinai and northern Britain. We classified both faults and joints as open, filled and partly filled (i.e. a granulation seam reactivated as an open fracture). We recorded, where possible, the fracture orientation, aperture or thickness, throw, surface striae, length, width, host lithology and geometric characteristics such as linkage with other fractures. In this article we consider only the data from faults, where we could measure offsets parallel to the fracture surface.

We estimated damage zone widths from fault frequency vs distance plots. In some cases, it was difficult to define a damage zone width, particularly where damage zones overlapped. Data presented in Table 1 come from isolated faults where the extent of the damage zone is clearly defined by the drop in fault density below a value of one fault per 10 m taken as a background value. Fault frequency for each traverse presented is divided into 10 m sections to indicate the lateral variation in fault density. For each traverse, minor structures were measured over a continuous section of outcrop from the start to the end of the traverse.

In northern England, we considered deformation associated with the Ninety Fathom fault, an approximately E–W-striking fault active during Carboniferous, Permian, Jurassic and Tertiary times (Jones 1967, Collier 1989) (Fig. 2). The fault has a present-day normal offset, but has experienced minor reverse reactivation (Collier 1989). The tensile and contractional fields around the fault will have been different for the extensional and reverse reactivation events. The dominant movement was during extension faulting. In a traverse normal to the fault across the Permian (?) Yellow Sands, a fine- to medium-grained aeolian deposit (Jones 1967) in the hangingwall, granulation seams are the dominant fault type. The great majority (>90%) of minor conjugate normal faults and granulation seams trend E–W, similar to the major fault, but a subordinate conjugate fault set trends roughly N–S (Collier 1989). Since nearly all faults have an E–W orientation, we infer that they constitute a single population. A fault-frequency plot (Fig. 3) shows that fault frequency per 10 m gradually diminishes away from the master fault. The damage zone probably continues beyond the outcrop in the exposure at Cullercoats (Fig. 2). The throw on the Ninety Fathom fault at this locality is approximately 140 m (Jones 1967). According to a structure map based on coal mine plans (Jones 1967) and cross-sections (British Geological Survey 1975), throw on the Ninety Fathom fault increases downwards at this locality, indicating that this traverse crosses the hangingwall extensional field.

In western Sinai, we completed continuous lateral traverses in the Nubian Sandstone across normal faults with throws from a few kilometres to tens of metres (Fig. 4). We could determine throw gradients on large faults (throw >100 m) only in those cases where outcrops on mountain-sides were accessible. The majority of large and small faults analysed trend NW–SE following the axis of the Gulf of Suez rift (Fig. 4). Robson (1971) and Knott *et al.* (1995) give an overview of the localities studied and these are shown in Fig. 4. Figure 5(a) is a fault-frequency plot compiled from a traverse across two faults. The fault on the right-hand side has a throw of 50 m. Throw increases downward, indicating that this part of the traverse crosses the hangingwall extensional field. Fault frequency per 10 m (granulation seams are the dominant structure) is greatest in the hangingwall of the large fault and diminishes away from the fault quite rapidly (Fig. 5a). In the footwall to this fault, damage is less intense with fault frequency decreasing away from it. A small antithetic fault (at left in Fig. 5a) accounts for local increase in fault density in the hangingwall of the antithetic fault.

Similar data are found in the rocks from a traverse in western Sinai which crosses a fault with throw of 100 m and throw increases down dip (Fig. 5b). Damage is most intense in the immediate hangingwall of the fault. A section of poor quality exposure in the hangingwall is partly due to erosion of the faulted sandstone. In the footwall, deformation is less intense and fault frequency gradually increases away from the master fault as another fault is encroached, just beyond the left edge of Fig. 5(b). The minor fault frequency is increasing within the hangingwall of this second fault, as the fault is approached.

A traverse across a fault with up to 2 km throw, which juxtaposes Nubian Sandstone Formation and Miocene conglomeratic limestone, shows that the most intense deformation is located in the footwall and is spread over roughly 200 m (Fig. 6a). Damage in the hangingwall is less intense, partly due to the hangingwall lithology being syn-tectonic fan deltaic sediments comprising resedimented limestone clasts. These rocks are less likely to have developed shear fractures and granulation seams than the high porosity Nubian Sandstone Formation, as the former were unlikely to form a stress-supporting framework at the time of faulting. The footwall damage zone is relatively narrow given the large fault throw. Fault throw most likely increases downwards, although there is no direct evidence for this. If true, then the footwall would be in the contractional field and the Nubian Sandstone in the hangingwall, in the subsurface, would have a much wider damage zone than the footwall.

A traverse across several faults within the Nubian Sandstone Formation (Fig. 6b) shows a preponderance of high fault frequency in the footwalls. At the left edge of the traverse, a fault with approximately 200 m throw has the most intense faulting in the footwall. To the right, the next three faults have throws of approximately 30, 1.5 and 75–100 m, respectively. Each fault has the greatest density of minor faults and granulation seams in the footwall. Each of these faults has throw decreasing downwards and therefore the footwalls are in the extensional field.

Fault throw

We compiled a fault displacement population (Marrett & Allmendinger 1991) from a sub-area within the western Sinai region; our data display a clear straight line trend with a slope of −0.34 (Fig. 7). Fault throw data were obtained from core and depth structure maps from the northern North Sea field. Throw data from the depth structure map were obtained from closely spaced traverses across the map oriented normal to the main fault trend (Walsh *et al.* 1994). Throw data from core were measured along traverses down the centre of cores. The data set from the northern North Sea field gives a very clear straight line segment on the population graph for the seismically derived throws (Fig. 8). The straight line trend between the seismic data and the data obtained from core has a slope of −0.39. No discernable limit of seismic resolution is observed from the seismically derived part of the data set. Commonly, there is a sudden shallowing of slope on such data sets marking the onset of truncation due to the limit of seismic resolution, usually around 25 m throw (e.g. Yielding *et al.* 1992). The absence of this truncation limit is probably due to the use of seismic attribute maps and geological common sense regarding fault geometry and linkages when the interpreter constructed the depth structure map.

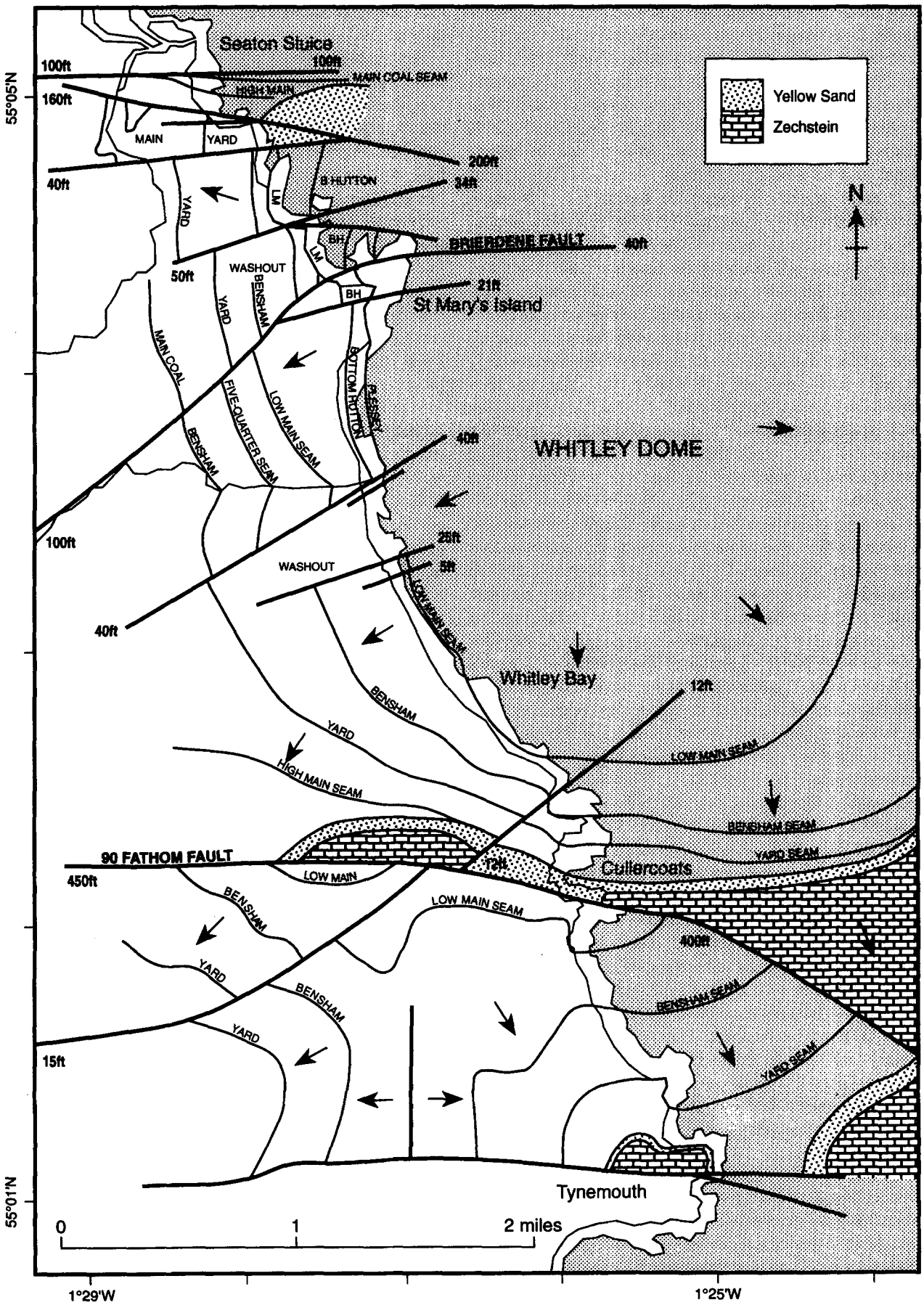

Fig. 2. Geological map of the Whitley Bay area, NE England and the Ninety Fathom fault. Unshaded—Carboniferous, black lines—coal seams, stipple—Yellow Sands, bricks—Zechstein evaporite, light grey shading—North Sea. Offshore geological data are based on coal mine plans. After Jones (1967).

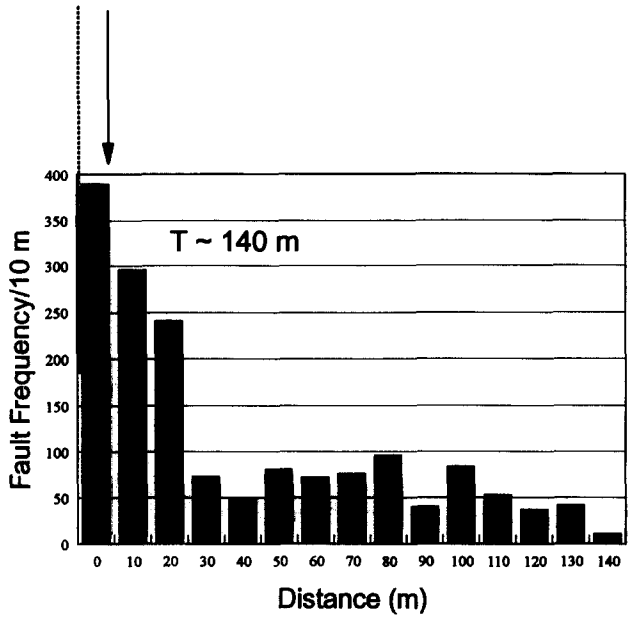

Fig. 3. Fault frequency–distance histogram across the Ninety Fathom fault hangingwall, Northumberland. Fault throw is approximately 140 m. Fault frequency per 10 m decreases in a direction away from the fault. Fault displacement increases downwards. All traverses are roughly orthogonal to fault strike. Vertical dashed line—position of fault, arrow—downthrown side, T—throw.

Fault length

Fault length data were collected from outcrops in western Sinai using a 1 m^2 grid laid on the outcrop. Only those fault lengths entirely contained within the metre square are plotted (Fig. 9). The graph indicates a clear, but very short, straight line segment with slope of −1.02. It is unclear whether this is statistically significant, as the straight segment spans less than one order of magnitude. It is most likely that this result is a measure of the dimension in which the sample was taken rather than anything specific about the fault length population itself (Yielding *et al.* 1996).

Fault length data from the subsurface depth structure map were taken from isolated faults only. Linked faults were ignored. Fault lengths from the map were measured to the nearest 10 m. Fault lengths were also measured from core and measured to the nearest mm. In order to plot the seismic and core data together, each fault length value from the depth structure map was divided by the surface area of the map and for the core, each fault length was divided by the total surface area of the core analysed. This data set gives a reasonably well-defined, straight central segment from the seismically derived fault lengths, and this trend lines up with the core data (Fig. 10). The slope of the trend is −1.29. Although the seismic and core data lie along the same trend, the absence of a clear straight segment on the seismically derived part of the data set makes this result a tentative one. Given the large gap between the seismically derived data and the core data, we cannot say for certain that there is a continuous spread of values in between. We discuss the evidence for gaps and clusters in such data sets in a later section.

Fault spacing

Fault spacings were measured from the Ninety Fathom fault outcrop at Cullercoats, Northumberland (Fig. 2). The plot of cumulative number vs spacing (Fig. 11) shows a clearly defined straight central segment with slope −0.63. A deviation from the straight segment at a spacing of roughly 2 cm could be attributed to truncation, i.e. not all closely spaced faults have been measured—perhaps micro-fractures would need to be included to fully characterize the population. However, the limit of measurement in the field was roughly 1 mm and it is believed that very few faults, visible to the eye, were missed. It is possible, however, through lumping together individual granulation seams into composite seams, that the smaller spacing values are undersampled.

An alternative interpretation of this result is that at close spacings, grain size becomes a significant factor in controlling fault growth. Generally, faults with small throws (1–10 mm) are closely spaced (10–100 mm) and when throw is of the same order of magnitude as the grain size of the sandstone, i.e. < 1 mm, then growth would be perturbed by grain rolling, grain boundary orientation and grain sliding (Aydin 1978, Knipe 1992). It is also possible that smaller spacings are less common due to tight clustering of faults as a result of increased porosity immediately adjacent to faults. These perturbations would affect the resulting fault characteristics and produce a deviation from the ideal fractal relationship.

Above spacings of 20 cm, a deviation from the straight line may also be due to the effect of truncation. It is likely that not all of the faults with larger spacings (>1 m) in the population have been measured and so an incomplete sampling of this part of the population may have been made. An alternative interpretation of the apparent non-linearity of spacing above 20 cm is that layer thickness is a controlling factor on fault spacing (Aviles *et al.* 1987, Okubo & Aki 1987, Pacheco *et al.* 1992, Wojtal 1994, Westaway 1994). By inspecting the original data, a spacing of 20 cm corresponds to a throw of roughly 0.6 m. Although it was not possible to measure maximum fault throws along the single line traverse in outcrop, throw can be approximately related to length through the displacement (D)–length (L) relationship:

$$D = BL^n \quad (1)$$

derived by Scholz & Cowie (1990) where $n = 1$ and B varies between 0.008 and 0.014 for an homogeneous lithology (Dawers & Anders 1995). Using this relationship and range of values for B gives a fault length of between 20 and 43 m. This range of fault lengths is close to the thickness of the Yellow Sands in this area, which is roughly 30 m.

It may be that the straight line segment on the spacing population graph (Fig. 11) represents only those faults with lengths less than roughly 30 m, i.e. those faults contained within the fairly homogeneous Yellow Sands.

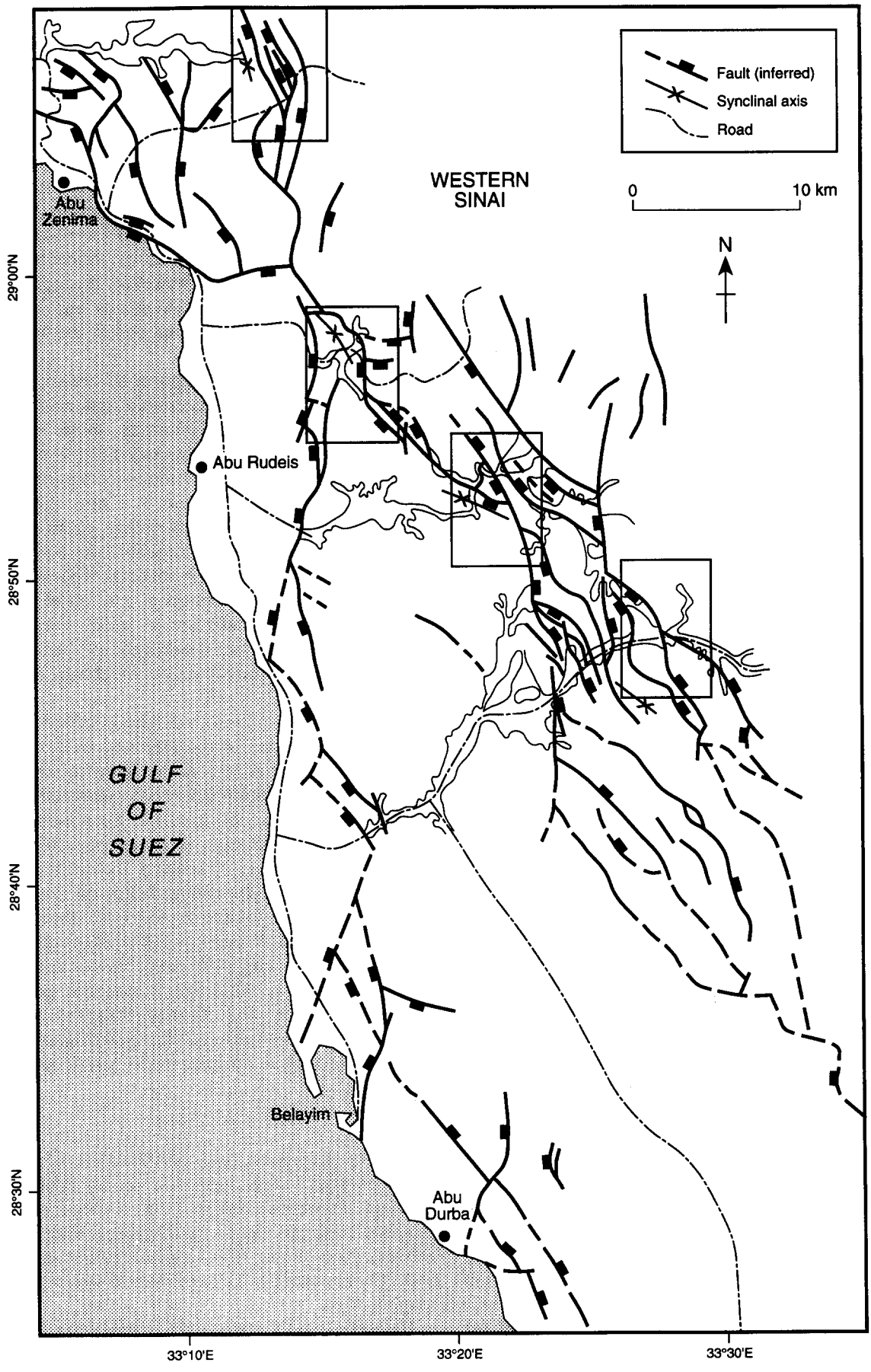

Fig. 4. Structural sketch map of western Sinai. Boxed areas indicate locations of detailed fault measurements and traverses. Based on Knott *et al.* (1995).

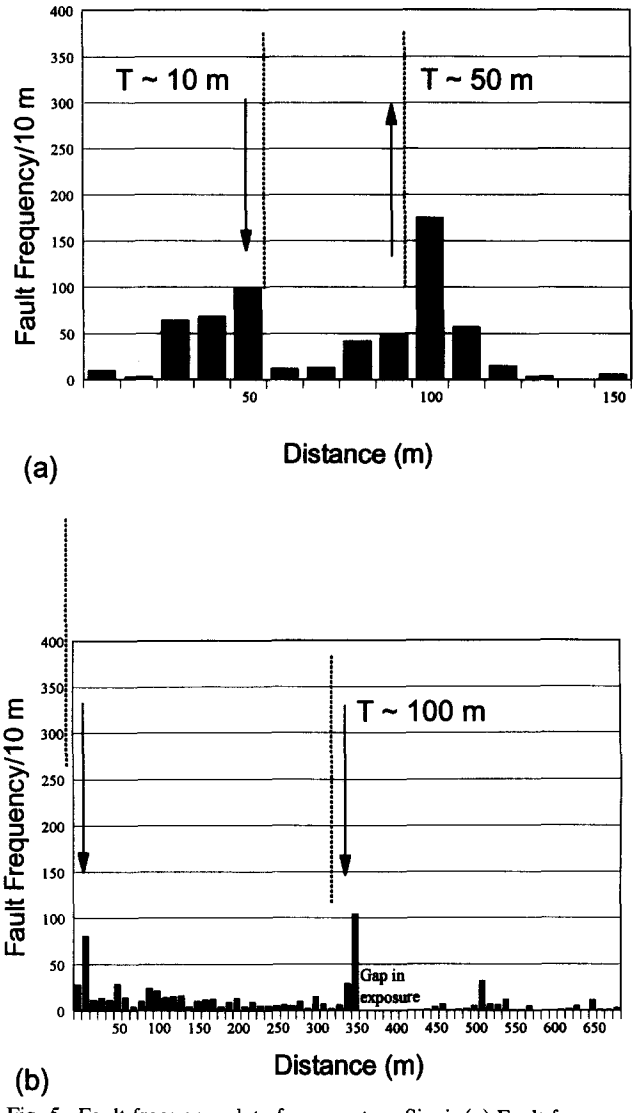

Fig. 5. Fault frequency data from western Sinai. (a) Fault frequency data across a normal fault within the Nubian Sandstone Formation with throw roughly 50 m with a minor antithetic fault on the left of the diagram. (b) Fault frequency data across a normal fault within the Nubian Sandstone Formation with throw roughly 100 m. Fault frequency per 10 m is greatest in the hangingwall and fault displacement increases downwards for each fault. Vertical dashed line—position of fault, down arrow—downthrown side, up arrow—upthrown side, T—throw.

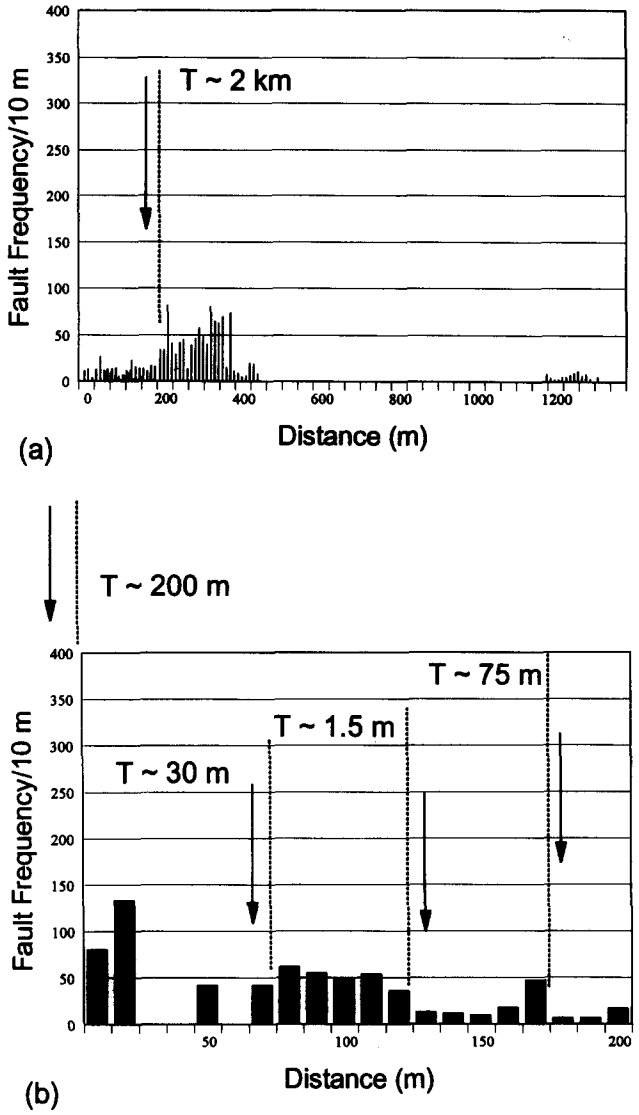

Fig. 6. Fault frequency data from western Sinai. (a) Fault frequency data across a normal fault juxtaposing Nubian Sandstone Formation in the footwall with Miocene conglomerate in the hangingwall. Throw is roughly 2 km. Fault frequency per 10 m is greatest in the footwall. It is predicted that the damage zone will be wider in the hangingwall Nubian Sandstone Formation. (b) Fault frequency data across four normal faults within Nubian Sandstone Formation with fault throws roughly 200, 30, 1.5 and 75–100 m respectively, from left to right. Fault frequency per 10 m is greatest in fault footwalls. Displacement decreases downwards on these faults. Vertical dashed line—position of fault, down arrow—downthrown side, up arrow—upthrown side, T—throw.

As soon as a fault propagated up into the dolomite and evaporite of the Zechstein Group, or downward into the shale and siltstone of the Carboniferous below, then its growth would be perturbed by the sudden change in lithology. Hence, the fault may no longer follow the same fractal relationship. Alternatively, faults with spacings >20 cm belong to a separate population that initiated outside the Yellow Sands, most likely within the underlying Carboniferous. It is proposed that the right-hand deviation from the straight segment could be an effect of layer thickness on fault growth and the resulting spacing population. The right-hand slope may still follow a power law but have a different exponent to the straight segment lying between 2 and 20 cm spacing.

The graph of spacing data from the northern North Sea depth structure map and core (Fig. 12) shows a clear straight line trend with slope of −1.31.

Fault zone thickness

Fault zone thickness data were collected from the same area in western Sinai as the throw data shown in Fig. 7, among other localities. Fault zone thickness is usually clearly defined as the zone where most fault slip has occurred and usually includes the slip surfaces and the band of fault gouge and cementation associated with cataclasis and fluid flow within the fault zone, respectively. We did not include undeformed blocks that had been entrained in the fault zone in our thickness measurements. In these cases, we measured each fault strand either side of the block separately. The fault zone is usually quite distinct from the damage zone. The

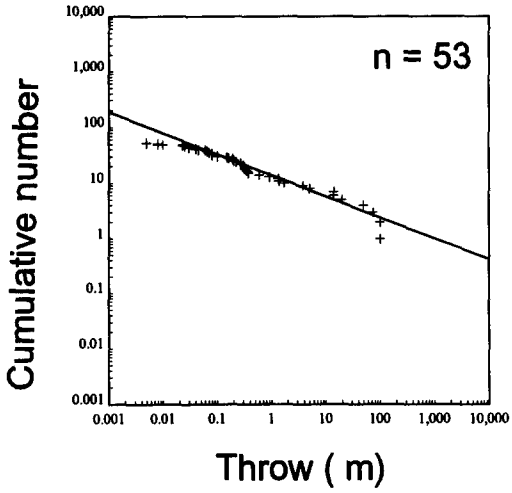

Fig. 7. Fault population graph of cumulative number vs fault throw from outcropping faults in western Sinai. The slope of the straight line trend on the graph is −0.34. The regression was carried out over the throw range 0.023–75 m. Correlation coefficient (r) = −0.49.

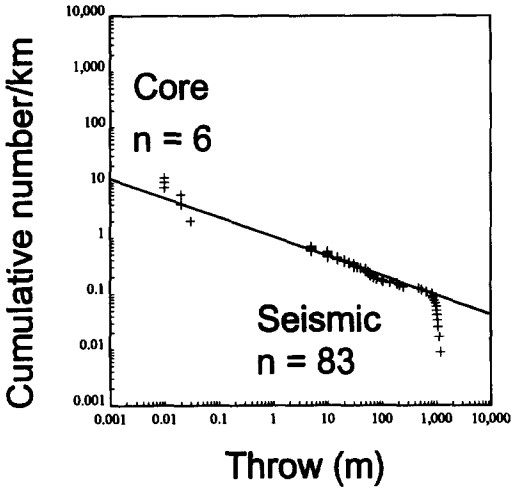

Fig. 8. Fault population graphs of cumulative number vs fault throw from subsurface seismic and core data for a northern North Sea field. Slope of straight line trend through seismic and core data is −0.39. The regression was carried out over the throw range 5–980 m. Correlation coefficient (r) = −0.64.

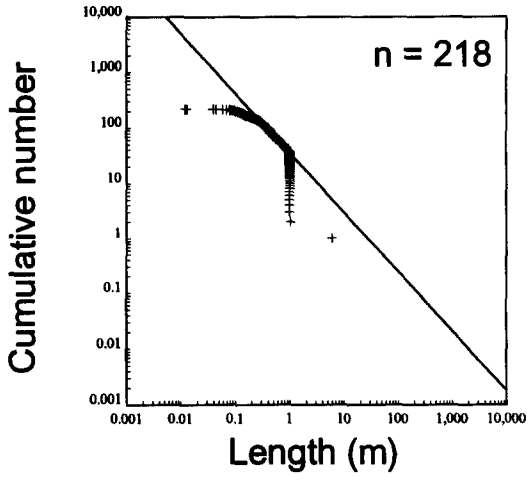

Fig. 9. Fault population graph of cumulative number vs length from outcropping faults in western Sinai. Lengths were measured from within a 1 m^2 grid. Faults that extended beyond the grid boundary were ignored. Slope of straight line trend is −1.02. The regression was carried out over the length range 0.31–0.93 m. Correlation coefficient (r) = −0.96. It is unclear whether this result is statistically significant, given that the straight line trend extends for less than one order of magnitude.

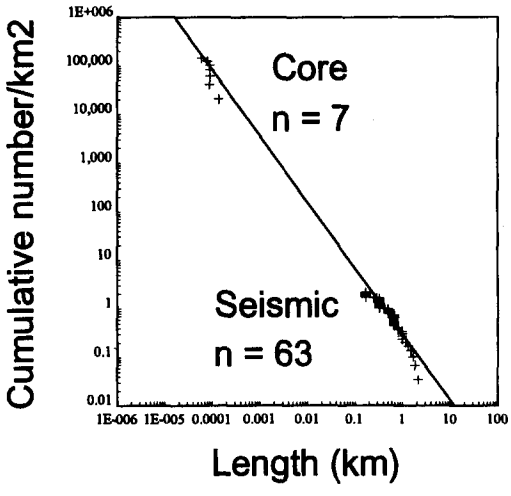

Fig. 10. Fault population graphs of cumulative number vs fault length from subsurface seismic and core data for a northern North Sea field. Slope of straight line trend through seismic and core data is −1.29. Regression was carried out over the length range 0.25–1.17 km. Correlation coefficient (r) = −0.92.

damage zone, as mentioned above, comprises the minor faults and granulation seams around a master fault and is much wider than the fault zone. Within the same lithology, fault zone thickness varies along the exposed trace of the fault length. Major variations in fault zone thickness occur when there is a change in lithology along the fault and also at fault jogs. The straight line slope on the thickness population graph (Fig. 13) is very clear and the slope is −0.32.

Throw and corresponding fault zone thickness data for all faults and granulation seams studied in the western Sinai region were plotted against each other in log–log space (Fig. 14a). A trend of slope close to one is obtained, with dispersion of points about this trend into bands broadly related to the different juxtaposed lithologies. Sandstone–shale juxtapositions lie towards the left-hand side of the trend and sandstone–sandstone juxtapositions lie to the right-hand side of the trend. Shale–shale juxtapositions are broadly scattered about the trend. The left-hand side of the plot shows the limit of resolution for fault zone thickness measurements at 1 mm. Juxtapositions involving sandstone and shale lie along a trend with thickness–throw ratio 1:100. Juxtapositions involving sandstone against sandstone lie along a trend with thickness–throw ratio 1:10. Very few data points lie beneath the line with thickness–throw ratio 1:1 (Fig. 14b).

The separation of the data on the basis of lithology is also an indication of the shear strength of the faulted rock types. The argillaceous lithologies have lower shear strengths than the coarse-grained sandstones and the former deform primarily by strain softening. Coarse-grained sandstones deform by strain hardening produc-

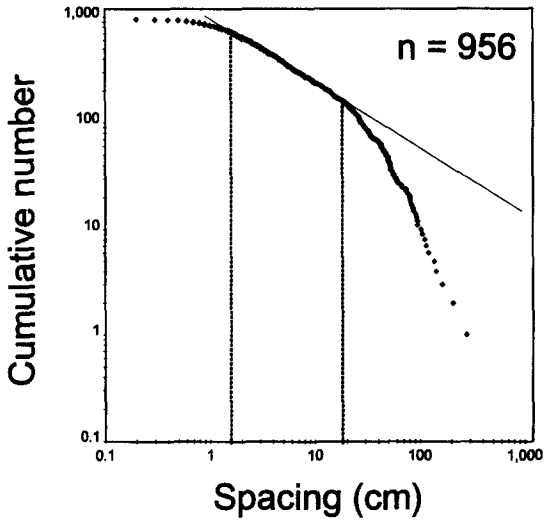

Fig. 11. Fault population graph of cumulative number vs fault spacing for the Ninety Fathom fault damage zone outcrop, Northumberland. Slope of straight line trend is −0.63. Regression was carried out over the spacing range 2–20 cm. Correlation coefficient (r) = −0.90. Deviation from the central straight line segment is marked by dashed lines at spacings of roughly 2 and 20 cm. See text for further explanation.

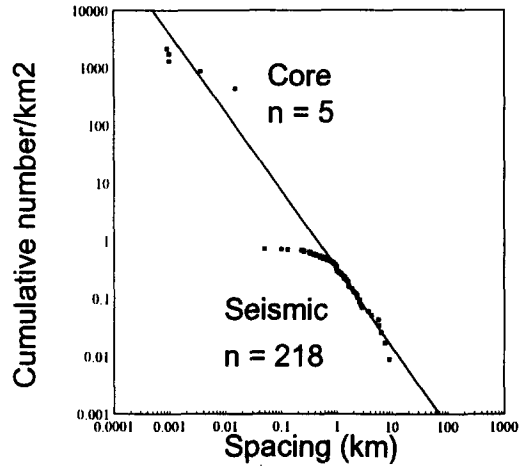

Fig. 12. Fault population graph of cumulative number vs fault spacing from subsurface seismic and core data for a northern North Sea field. Slope of straight line trend through seismic and core data is −1.31. Regression was carried out over the spacing range 0.8–7.45 km. Correlation coefficient (r) = −0.79.

ing granulation seams, for example (Aydin & Johnson 1983, Underhill & Woodcock 1987, Antonellini & Aydin 1994).

DISCUSSION

The outcrop and subsurface data sets described above sometimes support the general observation that populations of shear fractures have characteristics that are statistically self-similar over a range of sizes (King 1983, Watterson 1986, Yielding *et al.* 1992). Superimposed on this general observation are the effects of strain variation in the faulted volume, grain size, layer thickness and lithology.

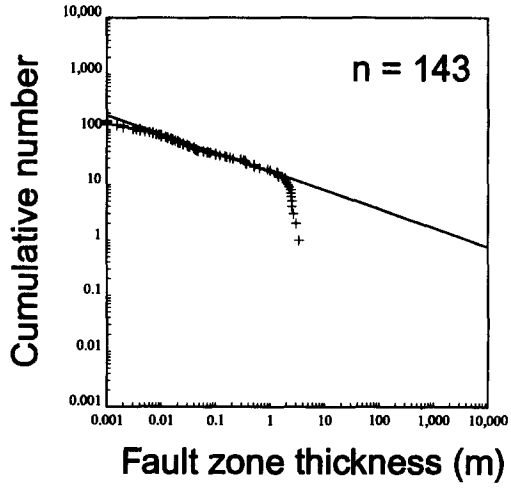

Fig. 13. Fault population graph of cumulative number vs fault zone thickness from outcropping faults in western Sinai. The slope of the straight line trend on the graph is −0.32. Regression was carried out over a thickness range of 0.01–1.97 m. Correlation coefficient (r) = −0.72.

Based on the outcrop data and due to the systematic variation in extension and contraction around a fault, a model of damage zone geometry has been produced. This model is derived in part from the geometries described by Muraoka & Kamata (1983) and Barnett *et al.* (1987) and data given in Table 1. The regularity of the relationship between fault throw and damage zone width compared with the broad scatter in the fault zone thickness data is mainly because damage zone widths were measured entirely within high porosity sandstones, whereas fault zone thickness was measured in sandstone, siltstone and shale.

In the extensional fields around an active normal fault, in the upper part of the hangingwall and in the lower part of the footwall, rocks are weakest because they are in tension, and minor faults and granulation seams form, reducing the effective permeability of the reservoir. From our outcrop observations, the extensional part of the damage zone is wider than the damage zone in the contractional field. The Ninety Fathom fault, Northumberland, displays one of the best exposed damage zones in Britain. The damage occurs mainly in the hangingwall in the tensile field, and fault frequency per 10 m decreases gradually away from the fault.

The formation of a damage zone of mesoscopic faults around a master fault is due to a combination of factors. These factors include quasi-plastic deformation at the fault tip as it propagates, and shear-related deformation due to accommodation of strain around a fault of variable slip. There are other factors which can contribute to the densities of mesoscopic faults around a master fault. Bends and relays along normal faults tend to be foci for mesoscopic fault generation (Peacock & Sanderson 1991). Fault jogs and local regions of either easy slip or fault sticking will also control minor fault distribution adjacent to a master fault (Platt & Leggett 1986). These additional processes will be superimposed on the effects of strain variation in the volume around the normal fault. We have not assessed the effects of strain harden-

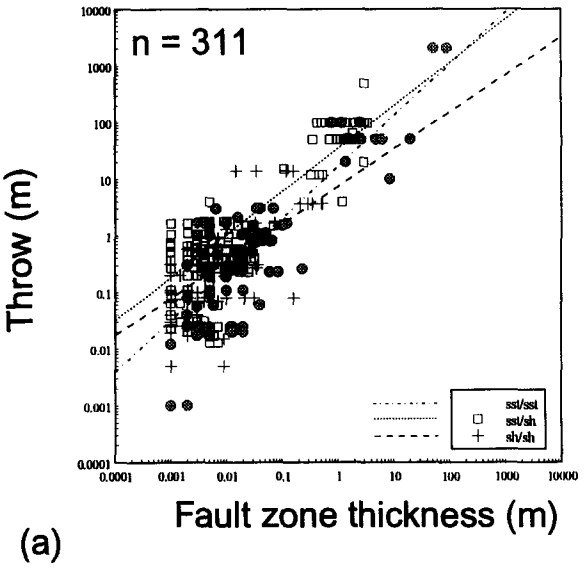

Fig. 14. Plots of fault throw vs fault zone thickness from faults in the Nubian Sandstone Formation outcropping in western Sinai. (a) Sandstone–sandstone juxtapositions lie along a line of slope 0.98 (r = 0.94). Sandstone–shale juxtapositions lie along a line of slope 0.83 (r = 0.70). Shale–shale juxtapositions show a broader scatter and lie along a line of slope 0.70 (r = 0.34). (b) The slope of the trend of all the data on the graph is approximately one. Sandstone–shale juxtapositions lie towards the left-hand side of the trend and sandstone–sandstone juxtapositions lie to the right-hand side of the trend. Juxtapositions involving sandstone and shale lie along a trend with thickness–throw ratio 1:100. Juxtapositions involving sandstone against sandstone lie along a trend with thickness–throw ratio 1:10. Very few data points lie beneath the line with thickness–throw ratio 1:1. See text for elaboration.

ing and softening, nor have we looked in detail at the effect of lithological variation on the width of the damage zone. We expect damage zones around strain softened faults in argillaceous sedimentary rocks to be relatively narrow compared with the damage zones we measured, which were exclusively within faulted high porosity sandstones as mentioned above.

We mapped fault damage zones onto subsurface depth structure maps using an empirical relationship between throw and damage zone half width derived in part from the outcrop data in Table 1 and from core and borehole image data from wells drilled within damage zones. Mapping of damage zones onto structure maps is based on the observation that damage zone half-width (i.e. on one side of the fault) is roughly twice the fault throw in the extensional field and is roughly half the fault throw in the contractional field. Examples of damage zones visible from seismic data have also been studied by us from unpublished commercial seismic data including seismic amplitude maps. We noted in our studies that the modelled damage zone envelopes corresponded closely to zones of noise within the seismic data and thus these zones of noise may correspond to the fault damage zones.

In the Ninety Fathom fault damage zone non-linear spacing at low spacing values (Fig. 11) is due to the effect of grain size on fault growth. For small fault throws (< 1 mm) fault growth is perturbed by grain sliding and rolling and the presence of pre-existing flaws. Once fault throws increase, then brittle processes dominate, including grain and cement fracturing, leading to growth of faults following a power law relationship.

As faults grew and propagated within the homogeneous Yellow Sands, they would continue to follow a power law relationship. Once the faults propagated outside the Yellow Sands, then their growth would be perturbed by penetration into a markedly different lithology. In the case of the Yellow Sands, the overlying and underlying lithologies are Zechstein Group dolomite and evaporite, and Carboniferous siltstone and shale, respectively. It is further speculated that the deviation of the larger spacing values from the fractal trend seen in the smaller spacing values from the Ninety Fathom fault damage zone corresponds to a separate population of larger faults that initially grew outwith the Yellow Sands. The larger faults could themselves follow a power law, but with a different exponent to the smaller faults.

The shallow slope for the smaller faults compared with the steeper slope for the larger faults is an indicator of the relative density of faults within each separate population. The difference in slopes is probably related to the extent of each population within the crust. The larger faults are relatively more numerous because that population is present over a much greater portion of the crust compared with the small faults which are contained within a distinctive layer of limited thickness such as the Yellow Sands.

The homogeneity of a layer depends upon the scale of observation. A distinctive part of a stratigraphic section can be considered homogeneous for faults of a particular size range. In western Sinai, the Nubian Sandstone Formation is a distinctive and laterally continuous layer sandwiched between overlying thick limestone and chalk, and underlain by basement (Robson 1971). In population graphs of fault throw data (Fig. 15a) and fault zone thickness data (Fig. 15b) from western Sinai, distinct gaps and changes in slope are evident which can be related to layer thickness. These gaps and changes in slope occur between 2 and 10 m, 20 and 40 m, and 100 and 200 m for fault throw (Fig. 15a), and between 0.1 and 0.3 m, 1.5 and 3 m, and 30 and 50 m for fault zone

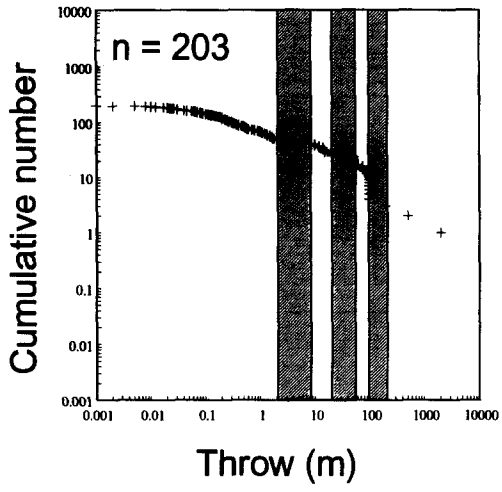

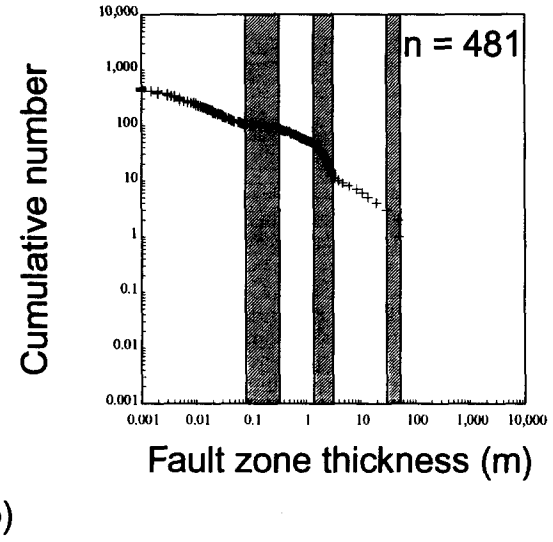

Fig. 15. Fault population graphs from faults outcropping in western Sinai. (a) Fault throw data as shown in Fig. 7. (b) Fault zone thickness data as shown in Fig. 13. Grey bands mark either gaps where there are notably fewer data points, or changes in slope of the population curve. Gaps occur at throw and thickness values that correspond to fault lengths of 300 m, 1500 m and 10 km. These values are close to the thickness of the distinctive mechanical layers within the western Sinai stratigraphy. See text for further explanation.

thickness (Fig. 15b). The gap in the larger fault zone thickness values is defined by only a few points, but is considered significant because of the corresponding gap in large throw values between 100 and 200 m.

Changes in slope could be due to sampling effects or rounding up to the nearest metre for example (Marrett & Allmendinger 1992, Walsh *et al.* 1994). However, in more recent fieldwork, we have carried out longer traverses attempting to identify faults with throws within the data gaps. Faults of these throw or thickness values were either rare or absent. Changes in slope on population graphs have been related to the temporal evolution of fault systems, including the effects of layer thickness, and this has led to the proposition that many fault populations are multi-fractal (Wojtal 1994). From the data presented here we indeed support this view.

Throw values in these gaps correlate with fault lengths

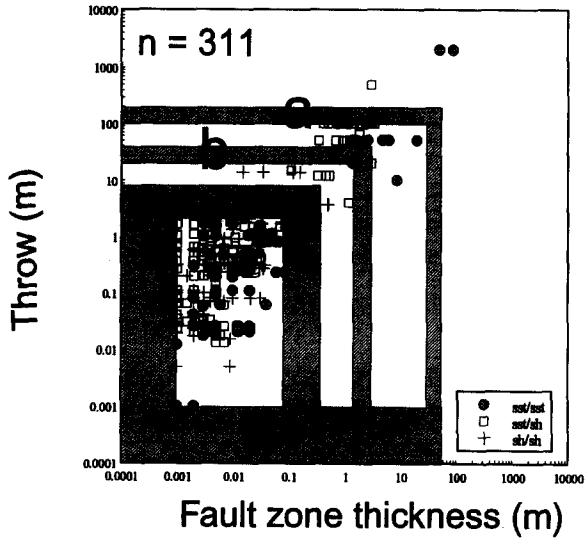

Fig. 16. Plot of fault throw vs fault zone thickness from faults in the Nubian Sandstone Formation outcropping in western Sinai. Grey bands are taken from Fig. 15. Band a marks a gap in data points which correspond to the thickness of the brittle crust in western Sinai (roughly 10 km, Steckler 1985). Band b marks a gap in data values corresponding to the thickness of the Nubian Sandstone Formation (roughly 1500 m, Robson 1971). Band c marks a gap in data values which corresponds to the thickness of the distinctive lower sandstone-rich part of the Nubian Sandstone Formation (roughly 300 m, Robson 1971). Band d is defined by the limit of resolution of outcrop measurements at 1 mm.

similar in size to the thickness of the key mechanical layers within the stratigraphy of western Sinai. The corresponding fault lengths would be roughly 300 m, 1500 m and 10 km, for maximum throws of 5, 20 and 150 m. These length values are similar, respectively, to the layer thickness of the lower sandy part of the Nubian Sandstone Formation (300 m, Robson 1971), the entire thickness of the Nubian Sandstone Formation (1500 m, Robson 1971) and the thickness of the brittle crust in the western Sinai region (10 km, Steckler 1985). It is proposed that the gaps and changes in slope in the population graphs are related to the thickness of the various mechanical layers within the western Sinai crust (Fig. 16).

A systematic relationship between throw and fault zone thickness has been defined similar to that documented by Hull (1988). When plotted in log–log space, the general throw-thickness trend shows a positive correlation with slope close to 1. The data are distributed about this trend systematically reflecting variation in the juxtaposed lithologies. Coarse sandstones have thicker fault zones for a given throw, due to the processes of strain hardening and cataclasis, compared with argillaceous rocks which are prone to strain softening. Although there is a general positive correlation between throw and thickness, thickness does not need to increase monotonically (Wojtal & Mitra 1986, 1988, Hull 1988, Evans 1990, Knott 1994). Sharp steps in the thickness–throw relationship are to be expected (Knott 1994) particularly for large faults (> 1 km throw) where strain softening is dominant (Hull 1988, Wojtal & Mitra 1986, 1988).

The fault formation mechanism proposed by Aydin (1978) and Aydin & Johnson (1978, 1983), where strain-

hardening shear bands precede fault development, provides a mechanical basis for fault zone thickening in high porosity sandstones (Underhill & Woodcock 1987, Antonellini & Aydin 1994, Knott 1994). The development of zones of granulation seams by this mechanism controls the location of the future site of the fault slip surface. The occurrence of high densities of granulation seams on one side of a fault or the other is apparently fortuitous.

CONCLUSIONS AND APPLICATION TO SUBSURFACE PROBLEMS

Each of the fault characteristics analysed are important for subsurface resource management. In this contribution, new evaluations of the process involved in fault growth and the effect of strain variation, layer thickness and lithology on normal fault populations have been presented. We have shown from our data sets that the assumption of a continuous self-similar relationship over all sizes of faults does not always hold in nature.

Damage zone widths can be related to fault throw and strain variation in the volume around a master fault. The damage zone widens with increasing fault throw and is widest in the tensile field of a normal fault, which could be in the hangingwall or the footwall depending on whether the upper or lower part of the fault is being examined, respectively. Faults on subsurface depth structure maps can be augmented with predicted damage zone envelopes once the calibration between fault throw, damage zone width, and lithology has been made either from outcrop or borehole image data.

Fault throw, length and spacing data from depth structure maps and core can show self-similarity over a range of scales and these results can be used to characterize the fault population below the limit of normal resolution (e.g. Yielding *et al.* 1992, Gaultier & Lake 1993). However, care must be taken when applying the results of such analyses, because fractal relationships sometimes do not hold for all ranges of fault sizes and effects such as layer thickness (Fig. 17) can cause fault characteristics to deviate from the ideal power law relationship.

Another practical implication of our analyses includes observations that fault zone characteristics including thickness, lateral continuity, gouge composition (cataclasite or shale smear), pore throat radii and permeability can be related to the sealing potential of a fault (e.g. Engelder 1974, Knipe 1992, Jev *et al.* 1993, Knott 1993, 1994, Hippler 1993, Lindsay *et al.* 1993, Edwards *et al.* 1994, Gibson 1994). A causal link has been proposed between fault throw, fault zone thickness and fault seal particularly in sandstone-rich successions where the fault seal membrane is provided by a low permeability cataclasite with small pore throat radii (Antonellini & Aydin 1994, Knott 1994).

A linear relationship between throw and fault zone thickness has been defined and scatter about this trend is primarily related to lithology and the mechanical properties of the host rock. Strain hardening is characteristic of porous sandstones (e.g. Underhill & Woodcock 1987, Antonellini & Aydin 1994) with thicker fault zones than argillaceous rocks, which are characterized by strain softening and thinner fault zones for the same throw (Knott 1994). The throw–thickness relationship can be used in fault seal prediction, because the thickness of the fault zone gives an indication of the likely lateral continuity of a fault rock sealing membrane along the fault surface. The throw–thickness relationship is also applicable to the estimation of fault transmissibility where fault zone thicknesses can be estimated from throws on depth structure maps, and lithology and fault zone permeability can be obtained from outcrop and well data to give transmissibilities for input to reservoir simulations.

Measurements of damage zone widths and fault zone thicknesses from borehole images and high resolution resistivity tools can be used to estimate fault throws using the above observations. This is particularly useful where resolution of complex fault blocks is difficult, especially on two-dimensional seismic reflection data, and the exact location of the wellbore within the seismic volume is uncertain.

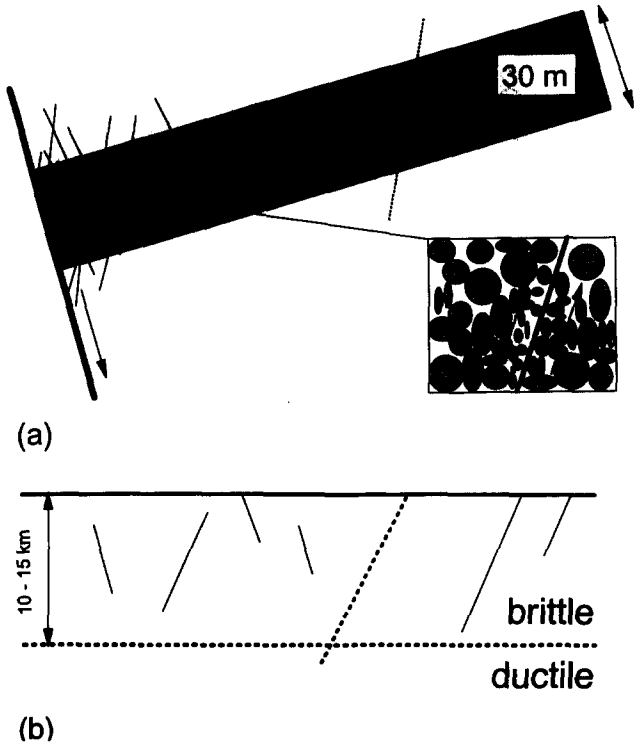

Fig. 17. Effect of grain size and layer thickness on fault populations. (a) Cartoon cross-section depicting the effect of grain size (see small box), and bed thickness on fault growth using the Ninety Fathom fault and Yellow Sands example. The fault population contained entirely within the Yellow Sands will have a consistent fractal dimension. Fault growth is perturbed as faults propagate out of the Yellow Sands upwards or downwards. (b) Cartoon cross-section of brittle and ductile crust. Faults that grow within the upper, brittle crust will have a different fractal dimension to faults that propagate through the brittle crust and into the ductile, aseismic layer (based on Westaway 1994). See text for elaboration.

Acknowledgements—We thank BP Exploration Operating Company for giving us permission to present the subsurface data, and Norsk Hydro and Statoil for giving us permission to present the outcrop data from western Sinai. Sincere thanks to Steven Wojtal and reviewers Conrad Childs and James Evans for helpful and constructive comments which improved the text and figures. Michelle Quinn, Barbara Bruce and Martin Kidd are thanked for preparing the figures.

REFERENCES

Antonellini, M. & Aydin, A. 1994. Effect of faulting on fluid flow in porous sandstones: petrophysical properties. *Bull. Am. Ass. Petrol. Geol.* **78**, 355–377.

Aviles, C. A., Scholz, C. H. & Boatwright, J. 1987. Fractal analysis applied to characteristic segments of the San Andreas fault. *J. geophys. Res.* **92**, 331–344.

Aydin, A. 1978. Small faults formed as deformation bands in sandstone. *Pure & Appl. Geophys.* **116**, 913–930.

Aydin, A. & Johnson, A. M. 1978. Development of faults as zones of deformation bands and as slip surfaces in sandstone. *Pure & Appl. Geophys.* **116**, 931–942.

Aydin, A. & Johnson, A. M. 1983. Analysis of faulting in porous sandstones. *J. Struct. Geol.* **5**, 19–31.

Barnett, J. A. M., Mortimer, J., Rippon, J. H., Walsh, J. J. & Watterson, J. 1987. Displacement in the volume containing a single normal fault. *Bull. Am. Ass. Petrol. Geol.* **71**, 925–937.

British Geological Survey, 1975. Geological map of Tynemouth—Sheet 15, 1:50,000 scale.

Chester, F. M. & Logan, J. M. 1986. Implications for mechanical properties of brittle faults from observations of the Punchbowl Fault Zone, California. Internal structure of fault zones. *Pure & Appl. Geophys.* **124**, 77–106.

Childs, C., Walsh, J. J. & Watterson, J. 1990. A method for estimation of the density of fault displacements below the limits of seismic resolution in reservoir formations. In: *North Sea Oil and Gas Reservoirs II* (edited by A. T. Buller *et al.*). Norwegian Institute of Technology, 309–318.

Collier, R. E. 1989. Tectonic evolution of the Northumberland Basin; the effects of renewed extension upon an inverted extensional basin. *J. geol. Soc. Lond.* **146**, 981–989.

Cowie, P. A. & Scholz, C. H. 1992. Displacement–length relationships for faults; data synthesis and discussion. *J. Struct. Geol.* **14**, 1149–1156.

Dawers, N. H. & Anders, M. H. 1995. Displacement–length scaling and fault linkage. *J. Struct. Geol.* **17**, 607–614.

Dawers, N. H., Anders, M. H. & Scholz, C. H. 1993. Growth of normal faults: displacement–length scaling. *Geology* **21**, 1107–1110.

Edwards, H. E., Becker, A. D. & Howell, J. A. 1994. Compartmentalisation of an aeolian sandstone by structural heterogeneities: Permo-Triassic Hope Sandstone, Moray Firth, Scotland. *Geol. Soc. Spec. Publ. Lond.* **73**, 339–365.

Engelder, J. T. 1974. Cataclasis and the generation of fault gouge. *Bull. Geol. Soc. Am.* **85**, 1515–1522.

Evans, J. P. 1990. Thickness–displacement relationships for fault zones. *J. Struct. Geol.* **12**, 1061–1065.

Fowles, J. & Burley, S. 1994. Textural and permeability characteristics of faulted, high porosity sandstones. *Mar. Petrol. Geol.* **11**, 608–623.

Gaultier, B. D. M. & Lake, S. D. 1993. Probabilistic modelling of faults below the limit of seismic resolution in Pelican field, North Sea, offshore United Kingdom. *Bull. Am. Ass. Petrol. Geol.* **77**, 761–777.

Gibson, R. G. 1994. Fault-zone seals in siliciclastic strata of the Columbus Basin, offshore Trinidad. *Bull. Am. Ass. Petrol. Geol.* **78**, 1372–1385.

Gillespie, P. A., Howard, C. B., Walsh, J. J. & Watterson, J. 1993. Measurement and characterisation of spatial distributions of fractures. *Tectonophysics* **226**, 113–141.

Heffer, K. & Bevan, T. 1990. Scaling relationships in natural fractures—data, theory and applications. *Soc. Petrol. Eng.* Paper No. 209819.

Hippler, S. J. 1993. Deformation microstructures and diagenesis in sandstone adjacent to an extensional fault: implications to the flow and entrapment of hydrocarbons. *Bull. Am. Ass. Petrol. Geol.* **77**, 625–637.

Hull, J. 1988. Thickness–displacement relationships for deformation zones. *J. Struct. Geol.* **10**, 431–435.

Jev, B. J., Kaars-Sijpesteijn, C. H., Peters, M. P. A. M., Watts, N. L. & Wilkie, J. T. 1993. Akaso Field, Nigeria: use of integrated 3-D seismic, fault slicing, clay smearing and RFT pressure data on fault trapping and dynamic leakage. *Bull. Am. Ass. Petrol. Geol.* **77**, 1389–1404.

Jones, J. M. 1967. The geology of the coast section from Tynemouth to Seaton Sluice. *Trans. Nat. Hist. Soc. Northumbria* **16**, 153–192.

King, G. 1983. The accommodation of large strains in the upper lithosphere of the earth and other solids by self similar fault systems; the geometric origin of b-value. *Pure & Appl. Geophys* **121**, 761–815.

Knipe, R. J. 1992. Faulting processes and fault seal. In: *Structural Modelling and its Application to Petroleum Geology* (edited by Larsen, L. M. *et al.*). *Norweg. Petrol. Soc. (NPF) Spec. Publ.* **1**, 325–342.

Knott, S. D. 1993. Fault seal analysis in the North Sea. *Bull. Am. Ass. Petrol. Geol.* **77**, 778–792.

Knott, S. D. 1994. Fault zone thickness versus displacement: results from Permo-Triassic sandstone outcrops in NW England. *J. geol. Soc. Lond.* **151**, 17–25.

Knott, S. D., Beach, A., Welbon, A. I. & Brockbank, P. J. 1995. Basin inversion in the Gulf of Suez: implications for exploration and development in failed rifts. In: *Basin Inversion* (edited by Buchanan, J. & Buchanan, P.). *Spec. Publs geol. Soc. Lond.* **88**, 59–81.

Koestler, A. G., Milnes, A. G., Olsen, T. S. & Buller, A. T. 1994. A structural simulation tool for faulted sandstone reservoirs: exploratory study using data from Utah and the Gullfaks field. In: *North Sea Oil and Gas Reservoirs III* (edited by A. T. Buller *et al.*). Norwegian Institute of Technology, 157–165.

Lindsay, N. G., Murphy, F. C., Walsh, J. J. & Watterson, J. 1993. Outcrop studies of shale smears on fault surfaces. *Intl. Ass. Sed. Spec. Publ.* **15**, 113–123.

Marrett, R. & Allmendinger, R. W. 1991. Estimates of strain due to brittle faulting: sampling of fault populations. *J. Struct. Geol.* **13**, 735–738.

Marrett, R. & Allmendinger, R. W. 1992. Amount of extension on "small" faults: an example from the Viking Graben. *Geology* **20**, 47–50.

Muraoka, H. & Kamata, H. 1983. Displacement distribution along minor fault traces. *J. Struct. Geol.* **5**, 483–495.

Okubo, P. G. & Aki, K. 1987. Fractal geometry in the San Andreas fault system. *J. geophys. Res.* **92**, 345–355.

Pacheco, J. F., Scholz, C. F. & Sykes, L. R. 1992. Changes in frequency–size relationship from small to large earthquakes. *Nature* **355**, 71–73.

Peacock, D. C. P. & Sanderson, D. J. 1991. Displacements, segment linkage and relay ramps in normal fault zones. *J. Struct. Geol.* **13**, 721–733.

Platt, J. P. & Leggett, J. K. 1986. Stratal extension in thrust footwalls, Makran accretionary prism: implications for thrust tectonics. *Bull. Am. Ass. Petrol. Geol.* **70**, 191–203.

Randolph, L. & Johnson, B. 1989. Influence of faults of moderate displacement on groundwater flow in the Hickory Sandstone aquifer in Central Texas. *Geol. Soc. Am. Abstr. Progr.* **2**, A242.

Robson, D. A. 1971. The structure of the Gulf of Suez (Clysmic) rift, with special reference to the eastern side. *J. geol. Soc. Lond.* **127**, 247–276.

Scholz, C. H. & Cowie, P. A. 1990. Determination of total geologic strain from faulting. *Nature*, **346**, 837–839.

Steckler, M. S. 1985. Uplift and extension of the Gulf of Suez, indications of induced mantle convection. *Nature* **317**, 135–139.

Underhill, J. R. & Woodcock, N. H. 1987. Faulting mechanisms in high porosity sandstones; New Red Sandstone, Arran, Scotland. *Spec. Publs geol. Soc. Lond.* **29**, 91–105.

Walsh, J. J. & Watterson, J. 1988a. Analysis of the relationship between displacements and dimensions of faults. *J. Struct. Geol.* **10**, 239–247.

Walsh, J. J. & Watterson, J. 1988b. Dips of normal faults in British Coal Measures and other sedimentary sequences. *J. geol. Soc. Lond.* **145**, 859–874.

Walsh, J. J., Watterson, J. & Yielding, G. 1994. Determination and interpretation of fault size populations: procedures and problems. In: *North Sea Oil and Gas Reservoirs III* (edited by A. T. Buller *et al.*). Norwegian Institute of Technology, 141–155.

Watterson, J. 1986. Fault dimensions displacement and growth. *Pure & Appl. Geophys.* **124**, 365–372.

Westaway, R. 1994. Quantitative analysis of populations of small faults. *J. Struct. Geol.* **16**, 1259–1273.

Wojtal, S. F. 1994. Fault scaling laws and the temporal evolution of fault systems. *J. Struct. Geol.* **16**, 603–612.

Wojtal, S. F. & Mitra, G. 1986. Strain hardening and strain softening in fault zones from foreland thrusts. *Bull. geol. Soc. Am.* **97**, 674–687.

Wojtal, S. F. & Mitra, G. 1988. Nature of deformation in fault rocks from Appalachian thrusts. In: *Geometries and Mechanisms of Thrusting with Special Reference to the Appalachians* (edited by Mitra, G. & Wojtal, S. F.). *Spec. Pap. geol. Soc. Am.* **222**,17–33.

Yielding, G., Needham, T. & Jones, H. 1996. Sampling of fault populations using sub-surface data: a review. *J. Struct. Geol.* **18**, 135–146.

Yielding, G., Walsh, J. & Watterson, J. 1992. The prediction of small-scale faulting in reservoirs. *First Break* **10**, 449–460.